Anisotropic superconductors in tilted magnetic fields

V. K. Vlasko-Vlasov,[1] A. Glatz,[1,2] A. E. Koshelev,[1] U. Welp,[1] and W. K. Kwok[1]
[1]*Materials Science Division, Argonne National Laboratory, Argonne, Illinois 60439, USA*
[2]*Department of Physics, Northern Illinois University, DeKalb, Illinois 60115, USA*
(Received 21 April 2015; published 8 June 2015)

We present images of magnetic flux structures in a single crystal of $YBa_2Cu_3O_{7-d}$ during remagnetization by fields tilted from the basal plane of the crystal. Depending on the magnitude and angle of the applied field, we observe anisotropic flux penetration along and across the in-plane field component and emergence of vortex instabilities resulting in modulated flux distributions. We associate the observed patterns with flux cutting effects and with tilted vortex structures intrinsic for layered superconductors. Time dependent Ginzburg-Landau simulations show preferential vortex motion across the *c* axis and reveal the flux structure evolution in anisotropic superconductors under tilted magnetic fields.

DOI: 10.1103/PhysRevB.91.224505 PACS number(s): 74.25.Uv, 74.25.Dw, 74.25.Ha, 75.60.Ch

I. INTRODUCTION

The magnetic response of type II superconductors beyond the flux-free Meissner regime is controlled by vortices—individual flux lines carrying single magnetic flux quanta [1]. Unlike imaginary field lines used to visualize the magnetic field orientation and density in free space, vortices in superconductors are real elastic strings that interact with structural defects, sample boundaries, transport currents, and each other. An intimate balance of these interactions yields a rich variety of vortex structures and defines basic superconducting (SC) properties that are important for applications, such as the superconductor's current carrying capacity, microwave generation capability, and sensitivity to external ac and dc electromagnetic fields.

In isotropic superconductors, mutually repelling vortices are continuous and tend to align with the field direction, forming a hexagonal lattice. However, in strongly anisotropic cuprates and other layered SC systems, they can be represented by segments of Josephson strings centered between strongly SC atomic planes and pancake vortices residing in the planes [2–5]. The coupling between the in-plane magnetized Josephson vortices and perpendicularly magnetized pancakes is attractive [6] and depends on the strength of the Josephson and magnetic interactions and on the magnitude and orientation of field. As a result, there is a large variety of novel vortex phases, including staircase or kinked vortices, crossing vortex structures, tilted vortex chains, and coexisting vortices of different orientations, which evolve from one to another through a series of vortex phase transitions (see [7] and references therein).

In addition to the variety of vortex structures, the SC anisotropy yields peculiar features in the field-vortex and vortex-vortex interactions. For example, the competition between the minimum vortex line energy [e.g., for vortices aligned with the cuprate planes in high-temperature superconductors (HTS) [8]], and coupling of vortices and the applied field $\mathbf{H}_a$, results in strong deformation of the vortex lattice unit cell and a large deviation of the vortex lines from the direction of $\mathbf{H}_a$ [9–12]. It can also lead to coexistence of different vortex orientations [13] or to sharp "lock-in" of vortices along the basal plane in layered materials [4,5,14]. Furthermore, the demagnetization effect due to the platelet shape, typical for anisotropic high-T_c crystals, introduces an additional constraint in the vortex orientation, confining them along the *c* axis or near the *ab* plane depending on the applied field direction [11,15]. Also, counterintuitively, the field of vortices tilted from the anisotropy axis becomes inverted at some distance from the core, causing the attraction of parallel vortices in the tilt plane and resulting in the formation of dense vortex chains within a dilute Abrikosov lattice [10,16,17]. Other intriguing features include the appearance of angular vortex instabilities and phase decomposition of the vortex matter in tilted magnetic fields [7,13,18–24]. Some of the above theoretical concepts, in particular, the formation of vortex chains in tilted fields and the attraction of pancake stacks to Josephson strings, were nicely confirmed by experiments. Comprehensive reviews of vortex behavior in layered HTS can be found in [5,25,26]. However, despite extensive experimental efforts, a larger part of the theoretically predicted vortex configurations in anisotropic superconductors still remains to be confirmed.

In this paper we study flux patterns in a high-quality $YBa_2Cu_3O_{7-\delta}$ (YBCO) crystal during remagnetization by fields tilted at different angles with respect to the basal plane. This is an extension of our previous studies of the same sample under crossing magnetic fields [27]. We reveal a large anisotropy of the vortex dynamics with preferential vortex motion along the *ab* plane. In tilted fields the in-plane flux component enters first, followed by tilted vortices carrying the normal component of the flux. The normal flux entry is accompanied by angular vortex instabilities, resulting in the modulated flux patterns. With increasing field angle, the normal flux forms smooth fronts advancing along the in-plane field component $H_{||}$ and sharp fronts slowly moving across $H_{||}$. The sharp vortex fronts carry strongly enhanced currents supporting flux cutting processes at the boundary between the in-plane and tilted vortices. At larger field angles and at increased fields, we observe qualitative changes in the vortex dynamics precipitated by the crossover from the staircase to the tilted vortex structure. We use time dependent Ginzburg-Landau (TDGL) simulations to model the flux evolution in anisotropic superconductors under tilted magnetic fields.

II. EXPERIMENT

A magneto-optical (MO) imaging technique [28] was used to study magnetic flux patterns in a high-quality optimally doped YBCO crystal with $T_c = 92.4$ K and the SC transition width $\Delta T = 0.3$ K. The sample is a 1130 (length) × 340

 ©2015 American Physical Society

(width) × 20 μm^3 (height) rectangular plate with a few twin lamellae at one corner. The crystal, covered with a garnet MO indicator film, was cooled in an optical cryostat, and images of the normal component of induction in the sample during and after application of a magnetic field were obtained using a polarized light microscope. The external magnetic field $\mathbf{H}_a$ with maximum amplitude of 2.1 kOe was produced by air cooled coils with a soft magnetic core which could be tilted with respect to the sample plane. Below we present magnetic flux patterns that emerge upon initial application of the field and during cycling tilted fields in opposite directions. The evolution of flux distributions in the sample will be illustrated for magnetic fields tilted towards the c axis from the direction parallel to the length or width of the sample.

III. RESULTS AND DISCUSSION

A. Magnetic fields tilted from the direction of long sides

When the magnetic field is parallel to the ab plane (tilt angle $\theta = 0$) and oriented lengthwise (H_Y) the normal magnetic fields emerge near the short edges perpendicular to H_Y [see bright and dark contrast in Fig. 1(a)]. These normal fields appear due to the screening of increasing H_Y as sketched in Fig. 1(c). They change polarity when H_Y is decreased, and the MO image reveals the stray fields of the trapped in-plane vortices [see the inverted contrast at the short edges of the crystal in Fig. 1(b)]. The in-plane flux enters the sample at relatively weak H_Y ($<$100 Oe) due to the small c axis currents defining the critical state in the finite plate geometry [27]. This agrees with the results of Ref. [29], where the c axis critical current in YBCO was found to be at least an order of magnitude smaller than that in the ab plane. An unexpected alternating H_Z contrast forms along the long edge of the crystal [see Fig. 1(b)] due to the bending of current lines on the side faces of the anisotropic YBCO crystal as sketched in Fig. 1(d) (see also Ref. [27]).

For small tilt angles of $\mathbf{H}_a$ from the ab plane ($\theta < 0.5°$) the flux patterns are very similar to those observed at $\theta = 0$, indicating the lock-in effect expected in layered cuprates for fields close to the ab plane when vortices align with the cuprate planes in order to minimize their condensation energy (see, e.g., [4,5,14]). For fields larger than the lower critical field and accounting for the platelet shape of the sample, the lock-in angle below which vortices are "trapped" in the ab plane is estimated as [Eq. (8.63) in Ref. [5]]:

$$\theta_L = 2n_{ab}\left(H_{c1}^c/H\right)[\ln(k\Lambda/\xi)/\ln(\lambda/\xi)]$$

where $k \sim 1$, $n_{ab} \sim L_c/L_{ab}$, with L_i being the sample dimensions along the c and ab directions, H_{c1}^c is the lower critical field along the c axis, $\Lambda = d/\varepsilon$ with CuO layer gap d and anisotropy parameter $\varepsilon(<1)$,$\xi = \xi_{ab}-$ coherence length, and $\lambda = \lambda_{ab}-$ penetration depth. Substituting $L_c = 20\,\mu$m, $L_{ab} \sim 400\,\mu$m, $H \sim H_{c1}^c$ and $d = 1.2$ nm, $\xi = 2$ nm, $\lambda = 120$ nm, and $\varepsilon = 1/5$ [30], for our YBCO crystal we obtain $\theta_L \sim 1.5°$.

A strong tendency for the in-plane arrangement of vortices at small fields moderately tilted from the ab plane is expected within the anisotropic London approximation, which neglects layering. For a thin anisotropic plate perpendicular to the anisotropy axis, the relation between the field angle (θ) and the vortex angle (Θ) with respect to the ab plane at fields $H_a \sim H_{c1}$ is cotan $\Theta = 2[(1-n)/(1+n)]\,\varepsilon^{-2}$ cotan θ [11]. Here n is the demagnetization factor, which for a thin ellipsoid with a short axis h and large axis w is $n = 1-(h/w)\pi/2$. Using $h = 20\,\mu$m and $w = 340\,\mu$m for our sample, we obtain cotan $\Theta \sim 2.3$ cotan θ, which indicates that at small θ vortices should be virtually confined in the ab plane.

Despite the above estimates, already at $\theta \sim 0.6°$ we observe strongly anisotropic penetration of the normal flux component B_Z, demonstrating the emergence of vortices tilted from the ab plane (see Fig. 2). At small fields (below ~140 Oe, not shown), we observe normal fields only at the short edges of the crystal, perpendicular to the in-plane component of $\mathbf{H}_a$,

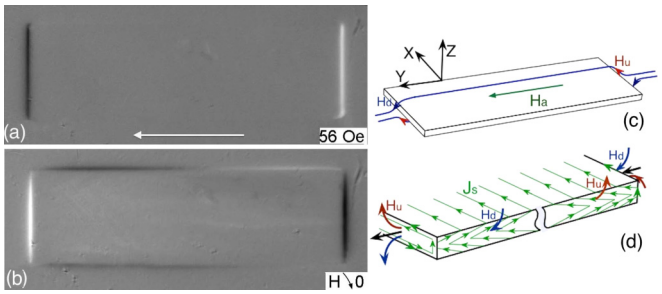

FIG. 1. (Color online) (a) Field patterns during applying and (b) after switching off (from $H_a^{max} = 2.1$ kOe) the longitudinal magnetic field parallel to the sample plane at $T = 50$ K. Field values are shown in the pictures. Bright and dark contrast corresponds to the up and down polarized normal fields, respectively. Schematics of magnetic field bending corresponding to partial field screening (a) and to the trapped in-plane flux (b) are shown in (c) and (d). Up and down polarized normal fields at the top surface are marked as H_u and H_d. The bending of the surface currents sketched in (d) explains the observed alternating contrast at the long sample edges in (b).

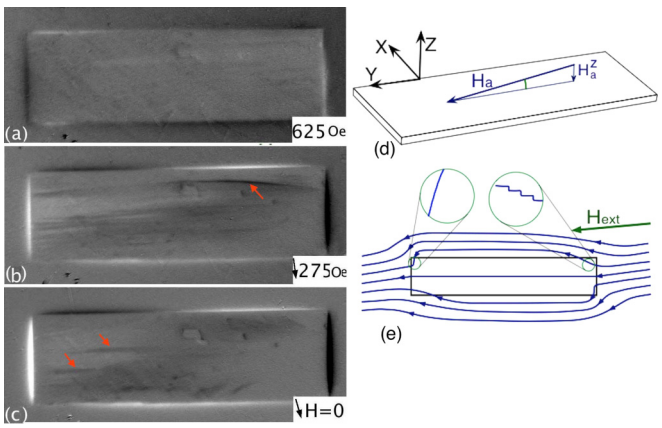

FIG. 2. (Color online) Field patterns in the increasing (a) and decreasing (b), (c) field tilted from the sample plane by 0.6° as shown in (d) obtained at $T = 50$ K. Small field images are identical to Fig. 1 and not shown. (a) Brighter streaks of penetrating B_z (of polarity opposite that of the applied field) stretch from the right short side with increasing H_a. (b), (c) Brighter streaks of B_z enter from the left short side after reducing H_a from $H_a^{max} = 2.1$ kOe. Horizontal lines of sharp contrast revealing increased currents along them are marked by arrows (b), (c). (e) Schematic explanation of the asymmetric B_Z entry shown in (a).

similar to Fig. 1(a). Note, that already at $H_a \sim 100$ Oe, in-plane vortices enter the sample, which is confirmed by the trapped flux image after successive reduction of the field to zero, similar to Fig. 1(b). However, if we increase the field above ~140 Oe, bright streaks carrying B_Z emerge from the right short edge of the crystal and propagate along the field direction with increasing H_a as shown in Fig. 2(a). Interestingly, the polarity of the penetrating $\mathbf{B}_Z$ in Fig. 2(a) is opposite to the normal component of $\mathbf{H}_a$ (bright contrast corresponds to $\mathbf{B}_Z$ pointing up). In this case, the direction of $\mathbf{B}_Z$ in the stripes matches the direction of the positive normal field at the right edge of the sample, induced by the screening supercurrents [see sketch in Fig. 2(e)]. We associate the observed asymmetric penetration of positive $\mathbf{B}_Z$ with different tilt angles of vortices entering from the opposite short sides of the crystal. With increasing H_a the normal field at the left edge, which is polarized along the negative H_a^Z [dark contrast in Fig. 2(a)], increases, tilting the edge field further from the ab plane. The positively polarized normal component of the field at the right edge should decrease, and the resulting edge field will tilt closer to the ab plane [see Fig. 2(e)]. At increasing H_a the field at the right edge tilted at a small angle to the ab plane, starts penetrating through the sample corners. This can be envisioned as the formation of staircase flux lines with pancake vortices, responsible for B_Z, easily propagating as kinks along Josephson-like strings inside the sample. Such staircase vortex structures are expected for layered YBCO in fields close to the cuprate planes [3,4,7,21]. At the left edge of the sample, the field tilt angle from the ab plane is larger, and the field should penetrate in the shape of tilted vortex lines, which experience stronger pinning and therefore are delayed. Although YBCO has moderate anisotropy, $\varepsilon^{-1} \sim 5{-}7$, the crossover from the three-dimensional (3D; tilted) to two-dimensional (2D; staircase) vortex behavior is expected below T_{cr}, which can be estimated using $\varepsilon^{-2}(1 - T_{cr}/T_c) = 2[\xi_{ab}(0)/s]^2$ [31]. For $\xi_{ab}(0) = 2$ nm and the distance between the CuO planes $s = 0.83$ nm, T_{cr} in YBCO will be ~51 K for $\varepsilon^{-1} \sim 5$ and 70 K for $\varepsilon^{-1} \sim 7$. Hence, the staircase vortex structure may exist in our sample. Direct Lorentz [32] and magnetic force microscopy (MFM) imaging of kinked vortices in YBCO [33] confirms such a possibility.

The weak B_Z stripes in Fig. 2(a) correspond to meandering supercurrent flow. It could be caused by imperfections along the short edges of the sample, resulting in the local suppression of the edge barrier for vortex entry. However, this assumption can be ruled out since no such imperfections were observed during normal field magnetization. A probable origin of the stripe flux structure could be vortex angle instability predicted for anisotropic superconductors in tilted fields [7,13,18–24]. The tilt of vortices near the right edges may fall into the range of angles for such instability. Another possible cause is helical perturbations expected when the in-plane currents induced by the normal component of $\mathbf{H}_a$ align with existing in-plane vortices. The helical deformation of vortices by longitudinal currents was proposed by Clem [34] and discussed later by Brandt [35] and Genenko [36]. Near the short edges of the sample, the screening currents are perpendicular to the longitudinal in-plane vortices, and the appearance of helical instabilities here would be unlikely. However, they can emerge further inside the sample, where currents flow lengthwise to the sample. This could explain the observed deep penetration of the B_Z stripes from the edges. Both angular and helical vortex instabilities should cause meandering of the current trajectories around their propagation direction and produce B_Z oscillations.

With *decreasing* H_a from 2.1 kOe the normal fields at the short X edges, which are caused by the in-plane trapped flux, invert, and the MO contrast switches intensities. Now stripes of positive B_Z asymmetrically stretch from the left edge [Fig. 2(b)]. Furthermore, lines of strongly increased currents revealed by the enhanced B_Z contrast [marked by arrow in Fig. 2(b)] appear along the in-plane field direction. The stripe flux structure with increased contrast indicative of filamented currents [see arrows in Fig. 2(c)] remains after switching off the field. These currents along the boundaries of the B_Z stripes support local twisting of vortices, which have different orientations in neighboring stripes.

Reversing the polarity of the initial tilted field as well as the change of direction of the tilt from the ab plane (up or down) qualitatively reproduces the same succession of flux patterns, with inversion of the normal fields at the short X edges and in the B_Z stripes. This is observed at all studied field angles. In all the figures we present sketches of the initial field orientation, which allows comparison of the emerging B_Z features with the normal components of $\mathbf{H}_a$ at different in-plane field directions.

At slightly larger tilt angles ($\theta \sim 1.5°$) and small fields, we observe the same dark and bright contrast at the short X edges as described above. However, at $H_a \sim 500$ Oe, a bright contrast forms around the entire sample perimeter. At these fields, the ab plane supercurrents screening the normal component of $\mathbf{H}_a$ become dominant. They enhance the normal field at the sample boundaries, as in the case of a purely perpendicular field applied to a SC plate. Further increasing the field to $H_a \sim 1000$ Oe results in the emergence of B_Z regions with smooth fronts in the shape of arches, expanding from the short edges and a sharp front of B_Z [marked by an arrow in Fig. 3(a)] entering from the top long edge. The sharp front is nearly parallel to the in-plane component of $\mathbf{H}_a$ and penetrates very slowly with increasing field. The contrast of the sharp front corresponds to the enhanced current along the boundary between the in-plane vortices in the central region and tilted vortices entering from the top long edge. We assume that the current enhancement is caused by the flux cutting process transpiring at this boundary. Similar fronts were observed during cross-field magnetization of YBCO [27]. The asymmetric formation of the sharp front is due to the difference in the edge barriers at the top and bottom long sides, which is revealed by magnetization in the perpendicular field [see Fig. 1(b)] in [27]. When decreasing the field from a maximum of $H_a = 2.1$ kOe, the sharp front spreads and merges with zones of weak B_Z expanding from the short edges [Fig. 3(b)]. After reducing the field to zero, the B_Z pattern transforms into bright longitudinal stripes [Fig. 3(c)] reminiscent of vortex domains with different tilt angles [37]. Also, dark and bright contrast due to the trapped in-plane flux appears at the short edges, and alternating contrast similar to that in Fig. 1(b) forms at the long edges. Note that bright B_Z stripes in Fig. 3(c) start at some distance from the right short edge. This is defined by the directions of the ab currents supporting the trapped B_Z and B_Y components, as shown in

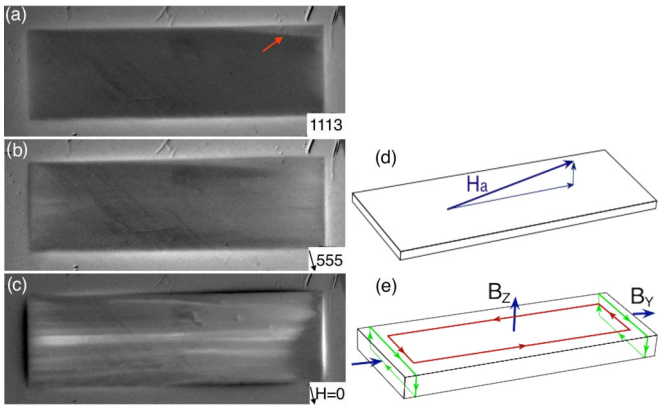

FIG. 3. (Color online) Flux entry (a) and exit (b), (c) in the external field tilted by 1.5° from the sample plane, as shown in (d), at $T = 50$ K. (a) Arrow points to a sharp B_Z front entering from the top long edge with increasing H_a. With decreasing H_a, positive B_z stripes [(b), (c), bright contrast] stretch along the in-plane component of the field. Bright and dark contrast at the short sides in (c) reveals the trapped longitudinal in-plane flux. (e) Sketch of currents supporting the B_Z and B_Y components of the trapped flux and responsible for the shift of the bright vortex domains away from the right short edge in (c). Modulations of the currents across the domains and enhanced currents along the domain walls are not shown.

the sketch of Fig. 3(e). At the right edge these currents are opposite near the top sample surface and compensate each other, leaving vortices in the ab plane instead of extending the B_z stripes to the right edge.

Tilting the applied field up to $\theta \sim 3°$ results in magnetization patterns similar to those observed for $\theta \sim 1.5°$ in the increasing field [Fig. 4(a); note that for the in-plane component of H_a indicated in Fig. 4(d) the sharp front marked by an arrow appears on the left, mirroring a similar front in Fig. 3(a)]. However, when we reduce H_a, the residual B_Z stripe structure transforms into a bow-tie pattern [Figs. 4(b) and 4(c)]. Also, alternating field contrast at the long edges of the crystal disappears, and the bright contrast at the left short edge weakens due to the circulating in-plane currents supporting

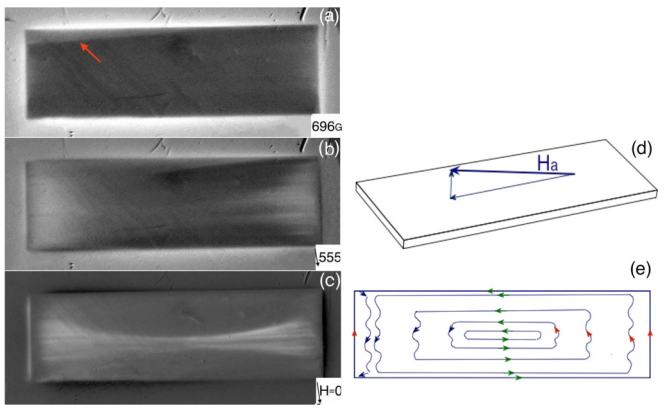

FIG. 4. (Color online) Flux entry (a) and exit (b), (c) in the field tilted by 3° from the sample plane, as shown in (d), at $T = 50$ K. The sharp front of B_Z is marked by arrow in (a). (e) Scheme of the current distribution corresponding to the bow-tie structure shown in (c).

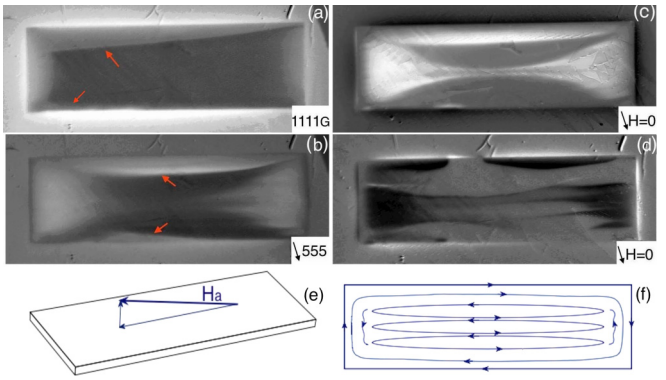

FIG. 5. (Color online) Flux patterns for increasing (a) and decreasing (b), (c) field tilted by 3.5° from the sample plane, as shown in (e), at $T = 50$ K. Sharp B_Z fronts are marked by arrows (a), (b). (d) Multiple bow-tie structures formed after successive application of a negative field of −2.1 kOe and after switching the field off. (f) Schematic of the current loops corresponding to (d). Reduction of the dark and bright contrast at the short sides (c), (d) is caused by the increased normal stray fields produced by the trapped B_Z.

the increased positive trapped B_Z. These currents enhance negative stray field around the sample.

We speculate that the bow-tie pattern in Fig. 4(c) is caused by strongly anisotropic in-plane currents associated with the anisotropic vortex dynamics. The advance motion of B_Z along the in-plane field component means that the average current density across the in-plane field component $H_a^{\parallel}$ is smaller than along $H_a^{\parallel}$, and the stripe B_Z structure corresponds to the oscillations of the transverse current lines as illustrated in Fig. 4(e). The stripes inside the bow-tie are very similar to the vortex domains reported in [37].

Increasing the field angle beyond $\theta \sim 3.5°$ induces the B_Z component entry at smaller values of H_a. Again, smooth arches of B_Z advance from the short edges while the sharp front moves from the top long edge and starts forming at the bottom long edge [Fig. 5(a)]. Upon reducing H_a the sharp fronts remain in place, and the ends of the bow-tie structure expand towards the corners [Figs. 5(b) and 5(c)]. After application of a negative field at the same angle, multiple bow-tie structures form instead of one [Fig. 5(d)], corresponding to several current loops stretched along the direction of the in-plane field component [Fig. 5(f)]. It was shown in [38] that the flux diffusion anisotropy induced by ac fields may cause the appearance of multiple current loops. In perpendicularly magnetized plates in the presence of a weak in-plane ac field, $\mathbf{H}_{\parallel}^{ac}$, the transverse critical currents (across $\mathbf{H}_{\parallel}^{ac}$) relax much faster than the longitudinal currents (parallel to $\mathbf{H}_{\parallel}^{ac}$). This results in the anisotropic reduction of flux gradients preferentially along $\mathbf{H}_{\parallel}^{ac}$, with the relaxation time inversely proportional to the ac field frequency and amplitude. Subsequent decay of the longitudinal currents near the sides aligned with $\mathbf{H}_{\parallel}^{ac}$ causes the reversal of the current flow and formation of additional current loops. Although we do not have ac fields in our experiment, but rather a slowly decreasing unidirectional field tilted at a small angle from the ab plane, the anisotropic flux relaxation with advanced motion of B_Z along the in-plane field component is expected from the

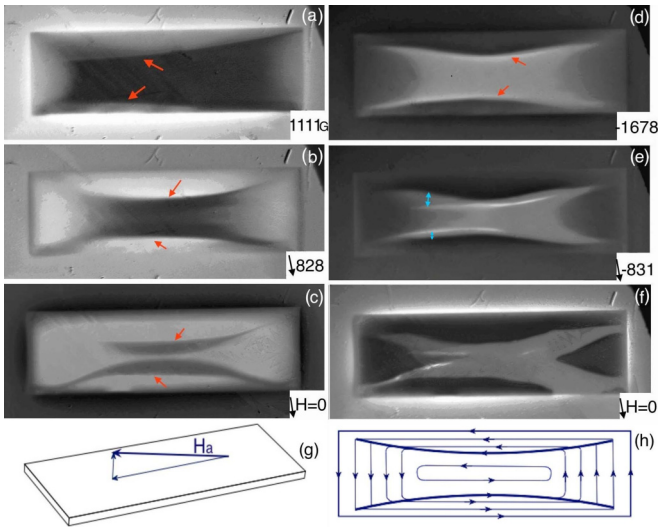

FIG. 6. (Color online) Flux patterns in the positive (a)–(c) and negative (d)–(f) tilted from the *ab* plane by 4° as shown in (g). Decreasing fields are marked by down arrows next to the H_a values. Images are taken at $T = 50$ K. Sharp B_Z fronts are marked by arrows (a)–(d). Splitting of the sharp fronts is indicated by double arrows (e). (h) Current scheme corresponding to the anisotropic vortex dynamics and formation of sharp fronts in (d). Bright and dark contrast at the short sides, expected for the in-plane trapped flux, is not visible in (c) and (f) due to the increased stray fields of the trapped B_Z.

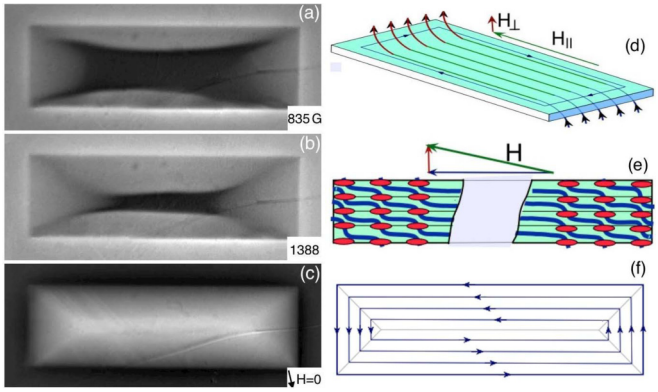

FIG. 7. (Color online) Flux patterns for increasing (a), (b) and decreasing (c) field tilted from the sample plane by 5°, at $T = 50$ K. (d) Schematic of the asymmetric tilt of vortices expected in Ref. [39]. (e) Symmetric entry of B_Z in the case of staircase vortex structure. (f) Sketch of the isotropic in-plane currents responsible for the envelopelike flux pattern in (c).

observed directional B_Z dynamics. It could be responsible for the formation of the current pattern sketched in Fig. 5(f).

At tilt angles above $\theta \sim 4°$, the opposite contrast at the short edges induced by the in-plane component of the field disappears at relatively small $H_a \sim 150$ Oe. With increasing field, sharp longitudinal fronts of B_Z form near the long edges, and the flux pattern becomes more symmetric [Fig. 6(a)]. Similarly, decreasing the field from 2.1 kOe, we observe a more symmetric picture of the sharp fronts penetrating deep into the sample and the bow-tie structure formed by smooth arches of B_Z extending from the short edges of the sample [Fig. 6(b)]. A qualitatively similar pattern but with negative normal stray fields (dark contrast) outside the sample is observed after reducing the field to zero [Fig. 6(c)]. In this state, the modulations inside the bow-tie structure are practically absent. Also, the contrast expected at the short edges due to the in-plane trapped flux vanishes.

Upon subsequent ramping of a *negative* H_a, both the sharp fronts and the bow-tie structure disappear, and new sharp fronts and smooth arches of *negative* $\mathbf{B}_Z$ enter the sample [Fig. 6(d)]. Currents along the front lines [marked by arrows in Fig. 6(d)] are strongly enhanced as revealed by the dark and bright contrast on their sides. Very similar flux patterns were observed during remagnetization of the sample by strong crossing fields [27]. When ramping down H_a from -2.1 kOe, the bright and dark contrasts at the sharp fronts split, leaving bright lines of positive B_Z in the crystal [Fig. 6(e)]. These lines correspond to boundaries between oppositely flowing currents and reveal the formation of new current loops in the sample. The bright lines break into segments and mostly disappear when switching off the field, while narrow wedges of negative B_Z form near the short edges [Fig. 6(f)]. Subsequent applying and switching off positive $H_a = 2.1$ kOe results in similar patterns but with inverted B_Z polarity in the wedges and regions near the long edges. Multiple current loops, as observed at $\theta \sim 3.5°$ [Fig. 5(d)], do not appear.

At tilt angles larger than $\theta \sim 5°$, arches of smooth fronts of B_Z propagating from the short sample edges and sharp fronts moving from the long edges enter deeper into the sample [Fig. 7(a)]. The smooth anisotropic propagation of B_z from the short edges is quite symmetric in contrast to the expected asymmetric entry [39] [Fig. 7(d)], which can be explained by the staircase structure of vortices as shown in Fig. 7(e). With increasing field, at $H_a \sim 1400$ Oe the B_Z fronts approach each other converging to an envelopelike pattern usually observed for purely perpendicular applied fields [Fig. 7(b)]. An inverted envelopelike pattern remains after switching off the field [Fig. 7(c)]. Such a B_Z distribution suggests that isotropic in-plane currents, which flow along the sample sides and make a sharp turn at the diagonals of the sample corners [Fig. 7(f)], become dominant. These currents support the normal trapped flux, while the in-plane flux component and appropriate *c* axis currents (see Ref. [27]) become inconsequential.

Thus in tilted fields, initially there is an easy entry of the in-plane vortices, which slide along the cuprate planes from the side faces of the YBCO plate. Starting with field angles of $\sim 0.5°$ from the *ab* plane, we observe the progressive penetration of the normal B_Z flux along the in-plane component of the field and restricted entry of B_Z across the in-plane field. At angles below $\sim 3.5°$ B_Z enters in the shape of narrow stripes aligned with the in-plane component of H_a, and after switching off the field, there is a noticeable component of the in-plane trapped flux. Increasing the angle above 3.5° results in the penetration of normal flux in the way of continuous fronts: smooth arches of B_Z easily advance from the short edges and move in the direction of the in-plane component of the field, whereas sharp B_Z fronts slowly enter from the long edges. At larger tilt angles, after switching off the field, the trapped normal flux supported by the *ab* currents dominates the picture. At tilts below $\sim 5°$, in-plane currents of the resulting trapped

critical state are strongly anisotropic, but at larger angles the trapped flux structure acquires a typical envelope pattern with isotropic in-plane currents parallel to the sample sides.

To understand the anisotropic tilted flux dynamics we will first analyze Brandt's model [25,39], which considers vortex motion in a long SC strip containing large longitudinal flux $B_{||}$ during application of the normal field $H_{\perp}$. The model predicts the advanced diffusivity of a relatively small normal flux along the in-plane $B_{||}$. The circulating currents screening $H_{\perp}$ flow along the long edges of the strip but are perpendicular to the longitudinal vortices near the short ends. At these ends, the in-plane vortices should start tilting from the sample plane, and from here $B_{\perp}$ will propagate along the strip as shown in Fig. 7(d). Vortices near the long edges are parallel to the screening currents and may be modified only by helical perturbations. According to [34–36] the right-handed vortex deformation in the force-free geometry ($\mathbf{J} \,||\, \mathbf{B}$) will start at the surface due to the tangential self-field of the current and shrink inside the sample. At the same time, left-handed helices excited in the interior will expand and compensate for the flux pumping from the incoming right-handed helices. Although these helical distortions are easily suppressed by pinning, they can be initiated in our sample due to currents induced by changing H_a.

In fields tilted from the long side, we observe stretching of the B_Z stripes from the short edges. Near these edges, screening supercurrents flow across the in-plane component of the applied field. The stripes have only one polarity coinciding with the B_Z direction at the neighboring edge. In contrast, helical vortices should yield lines with both positive and negative B_Z on their sides. Therefore, it is hard to directly associate the appearance of B_Z stripes with helical instability. Another possible explanation of the observed modulated flux structures is the angular instability of vortices tilted from the principle axis in anisotropic superconductors [7,13,18–24]. Recently we found that after cooling in a tilted field and slowly reducing the field, such an instability results in the formation of stripe domains containing vortices with different orientations [37]. We assume that the B_Z stripes observed during magnetization of the YBCO crystal at small θ is a precursor of the vortex domains caused by the same angular vortex instability. The instability causes inhomogeneous raising of the vortex tails near the short X ends, where the currents start meandering around the widthwise direction with a major wavelength of the developing angular instability.

The appearance of continuous fronts of B_Z at larger tilt angles (Figs. 5–7) has a different reason. As noted above, similar patterns form in the case of the normal field magnetization in the presence of a strong in-plane field [27]. Smooth B_Z fronts arching from the short sides along the $H_{||}$ direction are associated with the staircase structure of tilted vortices [3,4,7,21]. The in-plane component of the field, yielding Josephson-like vortices, easily penetrates along the cuprate planes from the side YZ faces of the sample at smaller fields because it is mostly screened by small c axis currents [27]. For layered bismuth strontium calcium copper oxide (BSCCO) crystals, the transparency to fields parallel to the cuprate planes is well documented and explains the experimentally observed sequence of parallel and then perpendicular flux entry in tilted fields (see Ref. [4] and references therein). The anisotropy of YBCO is much smaller, but early penetration of the in-plane flux in small crystals is expected. In our sample the easy entry of $B_{||}$ is confirmed by the appearance of stray fields due to the in-plane trapped flux observed at the short sides after applying and switching off a small tilted field. At increased fields, vortex pancakes slide along the Josephson vortex strings inside the sample. Therefore the normal component of the flux enters easier in the direction of $H_{||}$.

The sharp fronts formed at the sides parallel to $H_{||}$ outline boundaries between differently oriented vortices, where the flux cutting process occurs. It separates in-plane and tilted vortices during the initial magnetization and oppositely directed tilted vortices during remagnetization by negative H_a. The current along the front flows at some angle to the misaligned vortices surrounding the front and has a large component along the vortex lines. This current can be larger than the pinning critical current, which obstructs the transverse vortex dynamics. Motion of the sharp front is accompanied by the rotation of vortices due to vortex cutting and reconnecting events. The process of vortex cutting, when vortices experience strong local bending before collision, can introduce additional enhancement of the current [27]. The increased B_Z observed at the sharp fronts in our MO images is clear evidence of the locally enhanced current along these fronts.

At large tilt angles ($\theta \sim 4°$), during successive remagnetization by a negative field, the sharp fronts [Fig. 6(d)] should have a different structure compared with those formed at the initial application of the field. In YBCO plates remagnetized by perpendicular fields, the front is a flux-free cylinder (Meissner hole) formed by closed vortex loops, which collapse at a small radius due to the vortex line tension [40,41]. In the tilted field, one could expect a similar structure where the vortex loops surrounding the Meissner hole should strongly lean towards the ab plane as shown in Fig. 8. The front current will flow along $H_{||}$ at a small angle to the loops. It will yield a weaker Lorentz force on the side segments of the loops oriented close to the current direction and can be larger than the pinning critical current. This could explain the straight shape of the sharp fronts in tilted fields in contrast to wiggling Meissner holes formed by vertical vortex loops in the perpendicular field [40,41]. Note that top and bottom segments of the tilted

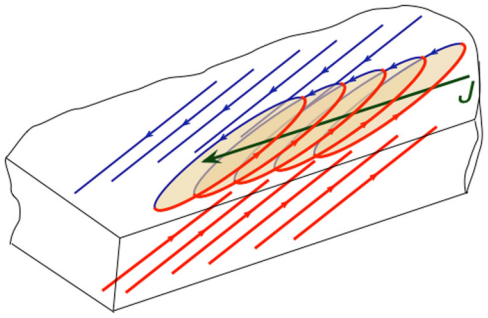

FIG. 8. (Color online) Sketch of the elliptical Meissner hole formed at remagnetization by the tilted field. The current along the Meissner hole (thick arrow) has a large component along the side segments of the vortex loops (thin arrows) and can be larger than the pinning critical current.

vortex loop are very close to the ab plane, and their line tension should be larger than for the tilted side segments [8]. As a result, the ellipticity of the tilted loops may be reduced.

For completeness of the picture, below we show flux distributions emerging in fields tilted from the widthwise sample plane direction.

B. Fields tilted from the direction of short sides

For the in-plane field (H_X) parallel to the short edges of the crystal, we observe MO patterns similar to those described above for the longitudinal field (H_Y) but rotated by 90°. With increasing H_X, normal magnetic fields (dark and bright contrast) appear at the long crystal edges. The contrast inverts after switching the field off due to the stray fields of the trapped in-plane flux.

Similar patterns defined mostly by the in-plane component H_a^X of the applied field are observed at small tilt angles of $\mathbf{H}_a$ ($\theta < \sim 0.4°$). At larger tilt angles, the effects of the normal component H_a^Z become noticeable. At $\theta = 1.2°$ and in small fields (~40 Oe), when the bright and dark contrast emerges along the long sides, a bright rim of enhanced normal field forms at the short sides [Fig. 9(a)]. The contrast in the MO image is caused by circulating in-plane currents induced by the z component of the applied field. At larger fields (~300 Oe) the effect of these currents becomes dominant, and enhanced positive normal fields (bright contrast) are observed around the entire sample perimeter [Fig. 9(b)]. Simultaneously, brighter wedges carrying a small B_Z component emerge from the lower long edge of the sample and advance in the direction of H_a^X. With increasing field, these wedges become narrower and transform into parallel stripes across the sample [Fig. 9(c)]. At this point, B_Z enters from the short ends and forms sharp fronts slightly tilted from the field direction. As in the case of longitudinal tilted fields, the enhanced current along these fronts is caused by the flux cutting process, which occurs at the boundary between in-plane vortices and successively entering tilted vortices. With increasing H_a, the sharp fronts advance very slowly while B_Z penetrates more efficiently from the long sides along H_a^X yielding a smooth flux gradient across the sample width [Fig. 9(d)]. Upon subsequent reduction of the field from 2.1 kOe, the normal flux exits near all the edges, keeping the stripe structure along H_a^X [Fig. 9(e)]. The sharp fronts of B_Z near the short sides initially remain in place and then smooth out. Finally, when the field is switched off [Fig. 9(f)], wider bright stripes of B_Z detached from the long edges and aligned with the short sides remain in the middle of the sample. They carry trapped positive B_Z, which produces negative normal stray fields (darker contrast) around the sample. The stripe structure represents vortex domains, where vortices are tilted at different angles from the sample plane as described in [37]. In addition to the stripes, we observe bright and dark contrast at the long edges due to the in-plane component of the trapped flux.

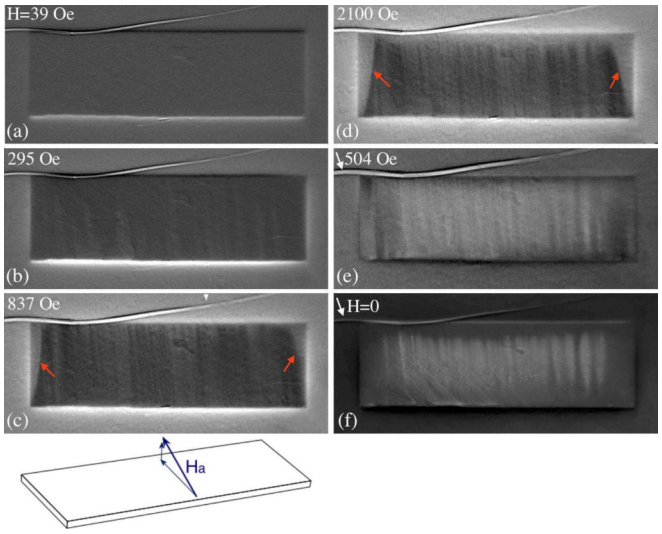

FIG. 9. (Color online) (a)–(f) Flux patterns in the transverse field tilted from the sample plane by 1.2°, as shown in (g), at $T = 50$ K. (a)–(d) Increasing and (e), (f) decreasing field. Sharp flux fronts in (c), (d) are marked by arrows. Note the qualitative similarity with Fig. 3 for small angle longitudinal fields.

Hence, the qualitative features of the vortex patterns in transverse tilted fields are similar to those observed for the longitudinal tilted fields. In both cases, at small field angles, the flux remains locked in the ab plane. With increasing field angle, stripe patterns of B_Z, caused by the angular vortex instability, stretch from the sides perpendicular to the in-plane field component $H_{||}$, and sharp flux cutting boundaries enter across $H_{||}$. At $\theta > 5°$, the flux structure transforms into envelopelike B_Z patterns characteristic of the normal field magnetization, suggesting the crossover from the staircase to the tilted vortex structure.

The effect of shape modifies the details of the patterns and conditions of their occurrence depending on the orientation of the tilted fields. For example, vortex domains are easily formed after ramping down the transverse tilted field, while they regularly appear only after field cooling in a certain range of angles of the longitudinal tilted fields [37]. In contrast, bow-tie structures always emerge with increasing tilt angles in the longitudinal tilted field geometry, but they are not observed in transverse fields. The differences are defined by the confinement of supercurrents in the finite-size rectangular plates, where c axis currents are much smaller than ab currents.

To clarify whether the SC anisotropy alone, without accounting for the layered structure, can be responsible for the specific features of the observed flux patterns, we modeled the remagnetization process in the tilted field using TDGL simulations. The results are presented in the following section.

IV. TDGL MODELING OF VORTEX DISTRIBUTIONS IN TILTED FIELDS

The TDGL equations were solved numerically in the large-λ limit using graphic card processing units as described in detail in Ref. [42]. In dimensionless units, the equation for the complex order parameter ψ is written as:

$$\partial_t \Psi + i\mu\Psi = \varepsilon(r)\Psi - |\Psi|^2\Psi + [g(\nabla - i\mathbf{A})]^2\Psi + \zeta(\mathbf{r},t)$$

with the scalar potential μ calculated self-consistently from the Poisson equation and vector potential $\mathbf{A}$. A thermal noise term ζ is defined by a correlator in coordinates $\mathbf{r}$ and time $t\langle\zeta(\mathbf{r},t)\zeta(\mathbf{r}',t')\rangle \propto T/T_c\delta(\mathbf{r}-\mathbf{r}')\delta(t-t')$,, where we choose

$T = T_c/2$. Tensor g describes the anisotropy of the SC parameters. In our case it rescales the gauge-invariant gradient in the z direction by a factor g, where $g = 5$ for YBCO. This corresponds to the alignment of the c axis in z direction. The model does not account for the layered structure of cuprates.

For the vector potential, we used the Landau gauge $\mathbf{A} = y[-B_z, 0, B_x]^T$. The unit of length is the zero-temperature coherence length $\xi_0 = \xi_{ab}$, the unit of time is the Ginzburg-Landau time $\tau_{GL} = \pi\hbar/8k_BT_C$, and the magnetic field is scaled to $B_{c2}(T = 0) = \Phi_0/2\pi\xi_0^2$. Also, we introduced weak quenched disorder $\varepsilon(r)$ to the system by slightly modulating the critical temperature at each grid point. The function $\varepsilon(r) = [T_c(r)/T] - 1$ is random in the interval [0.8, 1], which corresponds to a 10% modulation of T_c. The equation is discretized on a regular spatial mesh of 256 × 256 × 128 grid points with physical dimensions of 128 × 128 × $64\xi_0^3$ (i.e., the spatial discretization unit was $\xi_0/2$). The choice of this moderate volume allowed us to limit the calculation time, while at the same time realistically capture the dynamics of many interacting vortices. The minimum time step in our TDGL simulations was $0.1\tau_{GL}$.

To study peculiarities of the vortex dynamics in anisotropic superconductors and to clarify the role of the demagnetization effect, we implemented two sets of boundary conditions corresponding to different orientations of the sample surface with respect to the c axis. In one case the boundary conditions were chosen periodic in X and Z directions and open in the Y direction, which imitates large SC plates with XZ surfaces parallel to the c axis (||Z). In the other case, they were periodic in the X and Y directions and open in the Z direction, representing a large SC plate with XY surfaces perpendicular to the c axis. The TDGL equation was then solved using the implicit Crank-Nicolson scheme, which consecutively advances the state by one time step.

The system was initialized with a random state (arbitrary amplitudes and phases of the order parameter) and then relaxed in a magnetic field tilted from the X towards the Z direction by a small angle [$\mathbf{B}$ = (0.04, 0, 004)] for 80 000 time steps with relatively large noise for quick annealing. This created a dilute vortex lattice with clearly revealed individual vortices visualized by isosurfaces of $|\psi| = 0.5$. To study the remagnetization process, we gradually reduced $\mathbf{B}$ to 0 without changing orientation and then slowly increased the negative field with the same orientation to $\mathbf{B} = (-0.04, 0, -004)$.

A. XZ sample surfaces—SC plate with in-plane c axis

In the initial magnetized state, vortices are nearly parallel and aligned in the direction of the applied field (Fig. 10). The vortex cores are extended along the XY directions and are noticeably smaller in the Z direction due to the anisotropy. Vortices are bending more noticeably in the XY direction (perpendicular to the c axis) and tilt only slightly up and down from the field in the XZ projection. There is no distinct departure of the average vortex angle from $\mathbf{B}$ in contrast to predictions of [10–12]. This can be associated with the relatively large magnetic field of the initial state ($B \sim 0.04B_{c2}$), while the departure of vortices from $\mathbf{B}$ is expected at small fields. At the same time, bending of vortices in the XY projection can be associated with the effect of weak

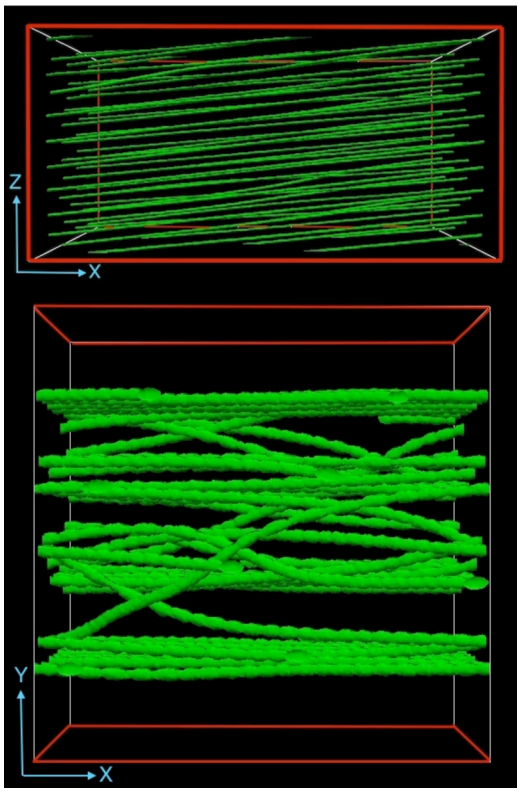

FIG. 10. (Color online) Projections of the simulated vortex configuration in the initial state at $\mathbf{B}/B_{c2} = (0.04, 0, 0.004)$ along Y and Z axes. XZ sample surfaces marked by red lines correspond to the extended plate with the c axis (||Z) in the plane of the plate.

disorder on the preferred vortex motion in the direction of the extended vortex core ($\perp c$).

Upon reducing and inverting the field, the vortices move towards the XZ surfaces, bend, and exit from the sample resulting in patterns shown in Figs. 11(a)–11(c) [left column]. The motion of vortices occurs basically in the planes nearly perpendicular to the Z axis. This preferential vortex diffusion along the ab plane caused by the anisotropy is in accordance with our experimental observations. Due to the pinning, a number of initially polarized vortices still remain in the sample at moderate negative fields. However, with increasing negative B, the total number of vortices essentially drops, and the remaining vortices rotate around the Z axis to the new field direction [Figs. 11(c) and 11(d)), left]. The process of the vortex rotation is illustrated in more detail in Fig. 12. Such a rotation of individual vortices in the plane perpendicular to the sample surface during the field reversal was not expected in existing models of remagnetization of superconductors. Some of the vortices repolarize by bending into loops, which then twist by moving their ends in opposite directions at the surface (Fig. 13). As soon as the motion occurs in close planes nearly parallel to the ab plane, the loops form very sharp twists, unusual for elastic vortex lines [Fig. 13(c)]. However, the sharp twists occur along the c axis, because the line tension for vortex segments along this direction is much smaller than for those aligned with the ab plane, as predicted in [8].

With further increasing negative B, loops of new negatively polarized vortices enter from the XZ surfaces [Fig. 11(e),

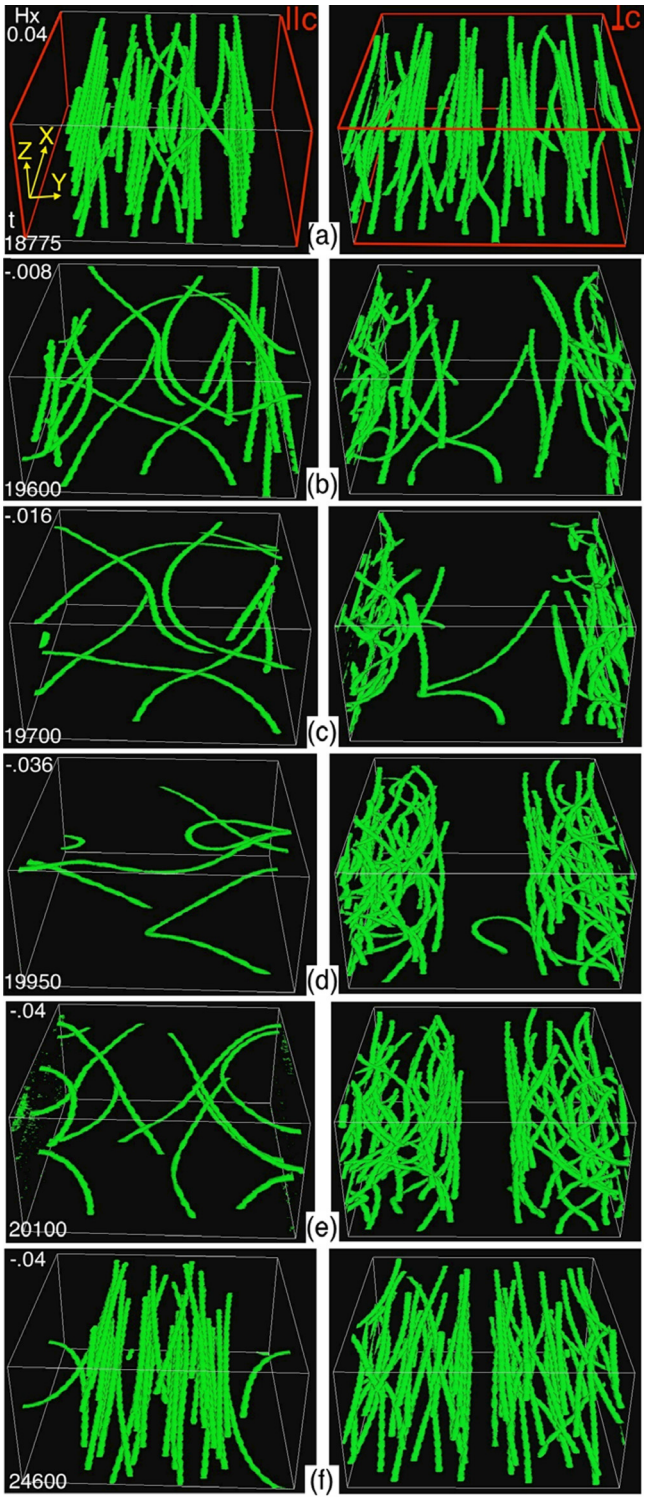

FIG. 11. (Color online) Vortex configurations during reversal of the tilted field. Left column corresponds to a plate with XZ surfaces ($||c$). Right column depicts a plate with XY surfaces ($\perp c$). $B_X/B_Z = 10$. Values of B_X/B_{c2} and time in τ_{GL} units (same for left and right columns) are shown on the panels.

left]. They also propagate preferentially in the Y direction in the planes nearly perpendicular to Z. They straighten and accumulate in the middle of the sample, aligning with the field direction, and form vortex-free zones near the surface

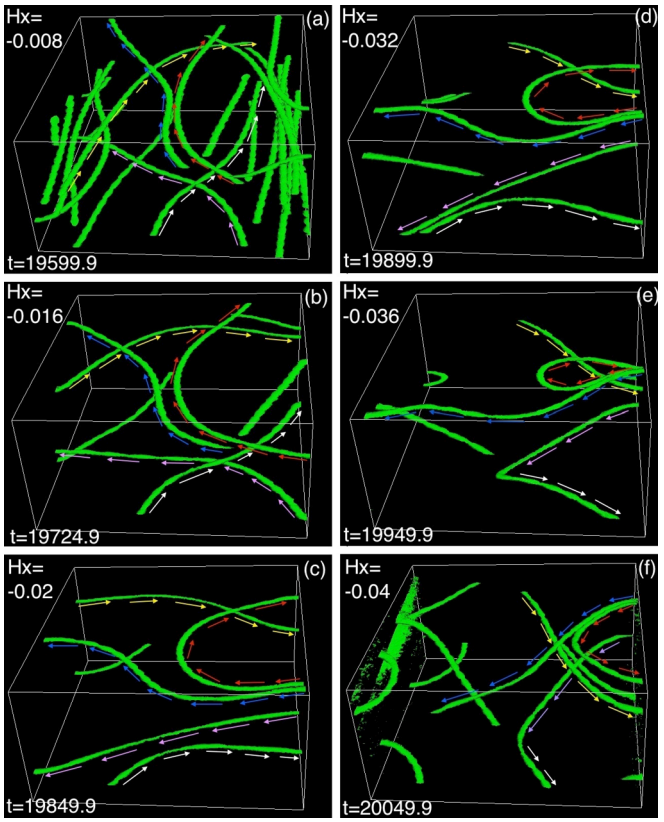

FIG. 12. (Color online) Changing vortex polarity due to the vortex rotation and twisting in the plate with XZ surfaces. $B_X/B_Z = 10$. Values of B_X and t are shown on the panels.

[Fig. 11(f), left]. This picture is reminiscent of the Bean-Livingston scenario in the case of weak pinning, when vortices, once they enter, are pushed from the surface by the Meissner currents.

B. XY sample surfaces—SC plate with perpendicular c axis

This geometry should account for the demagnetization factor $n \sim 1$ perpendicular to the plate. To see the difference introduced by the demagnetization effect, we show in the right column of Fig. 11 snapshots of the vortex configurations for XY surfaces at the same time and field values as in the left column. As in the previous case for maximum positive field, vortices with elliptic cores bend more easily in the ab plane than in the ac plane (Fig. 14). A clear tilt of the vortex ends near the XY surfaces towards the Z direction (i.e., towards the c axis). It is defined by the flow of supercurrents only parallel to the XY surface near the vortex ends.

Already in the initial state [Fig. 11(a), right] vortices are distributed more evenly in the Y direction compared with Fig. 11(a) (left) due to the absence of the surface barrier on the XZ faces. Another interesting feature is an apparent periodicity of the vortex density in Fig. 11(a) (right). Although disturbed by the structural disorder introduced in the simulations, vortices tend to form a lattice with a large period in the Y direction and with short intervortex distance along the Z axis. Such a stretched vortex unit cell is expected for fields close to the ab plane in anisotropic HTS [9–12]. A tendency

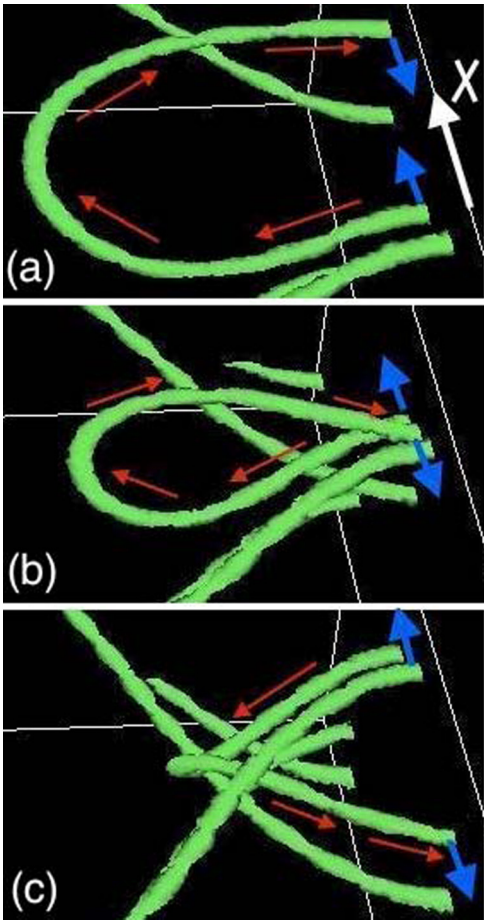

FIG. 13. (Color online) Reversal of the vortex loop chirality via the twisting of loop ends in the plate with XZ surfaces. The motion directions of the loop ends are shown by thick arrows (a)–(c). A sharp twist in (c) later untwists to form a vortex polarized along the negative field.

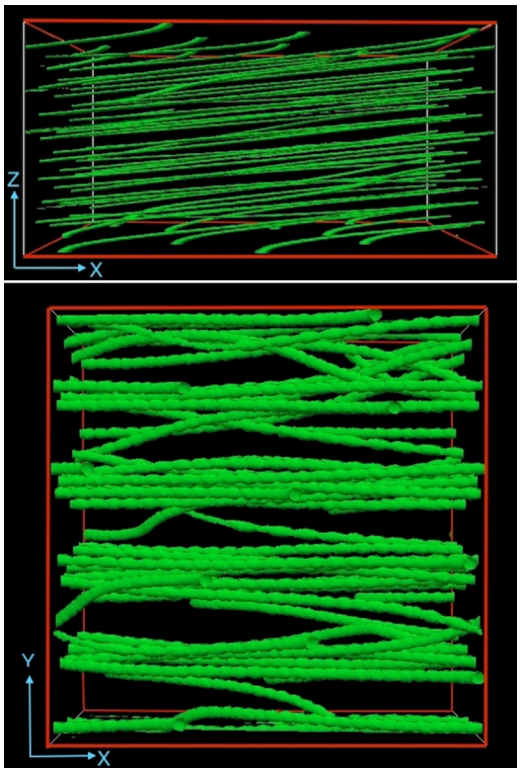

FIG. 14. (Color online) Projections of the initial vortex configuration along Y and Z axes in the plate with XY surfaces ($\perp c$) at $\mathbf{B} = (0.04, 0, 0.004)$ and $t = 18\,775\ \tau_{GL}$. Plate surfaces are marked by red lines.

towards periodicity along the Y axis can also be observed in Fig. 11(a) (left). In both cases, ordering of vortices in the ab direction is distorted by pinning (compare Figs. 10 and 14), but the average distance along the Z axis seems to be preserved.

With decreasing positive field followed by increasing negative field, vortices move preferentially in the Y direction [Fig. 11(b), right]. They do not escape from the sample through the XY surfaces of the plate but stay close to the ab plane and move perpendicular to the c axis. Some of the vortices bend, cut, and reconnect, forming loops, which twist and collapse. Interestingly, long oppositely polarized segments of neighboring vortices do not annihilate over an extended length but rather cut at one point (Fig. 15). The resulting sharp twists around the c axis formed at the ends of the cut move apart, yielding a straight vortex line polarized along the direction of the external field. At larger fields, new bent vortices with negative polarity enter from the right and left sides and not from the top and bottom plate surfaces [Fig. 11(c), right]. They collapse with the remaining positively polarized vortices and successively entering negative vortices advance in the Y direction, forming a front with a central flux-free area [Figs. 11(d) and 11(e), right]. This front propagates towards the sample center, and vortices straighten along the field and tend to order at larger B [Fig. 11(f), right].

Considering that the right column in Fig. 11 illustrates a large plate with XY surfaces, the nucleation of new vortices at the right and left sides of the simulated volume in Figs. 11(c)–11(f) (right) rather than at the top and bottom sample boundaries seems to be an artifact. It could result from the periodic boundary conditions, which impose a requirement on the order parameter, $\psi(x, 0, z) = \psi(x, L_Y, z)\exp[\Omega(B, x, t)]$, with 0 and L_Y boundaries of the simulation volume in the Y direction (see Ref. [42]). The phase factor Ω is strongly changing at the stepwise variations of B introduced by the numerics and causes an imbalance that can be restored only after an extended relaxation time. This imbalance yields strong ψ excitation on the left and right boundaries, resulting in the nucleation of vortices. In spite of the possibly artificial nature, this nucleation corresponds to our real experimental situation, where the sample is finite in the Y direction and vortices are initially entering from the narrow side faces of the plate. To test the effect of the boundary conditions, we repeated the simulations with the extended Y size of the sample ($256 \times 512 \times 128$). Due to the advanced vortex motion along the ab direction, this did not introduce any qualitative changes to the remagnetization process.

Summarizing, the simulations in both geometries confirm the preferential motion of tilted vortices along the ab plane in accordance with the experiment. The unexpected result is the rotation of vortices across the plate towards the negative field

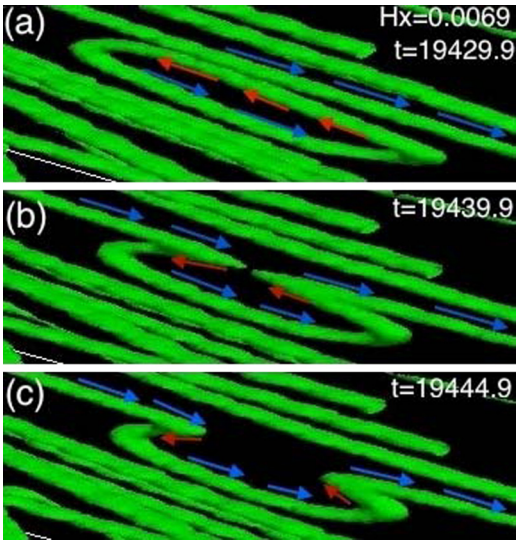

FIG. 15. (Color online) Collapse of antiparallel vortices in the plate with XY surfaces. Oppositely polarized segments of the stretched loop and the straight vortex (a) annihilate at one point (b), and the resulting two sharp vortex twists move apart (c). $B_x/B_z = 10$. (a) B_x is reduced from 0.04 to 0.0069 and does not change in the displayed time interval.

direction in the case of XZ surfaces (plate with the in-plane c axis). It does not appear in the case of XY surfaces (perpendicular to the c axis). A possible explanation is that for the XY surfaces, the simulations imitate a plate extended in the Y direction, and the rotation is more energy costly. The simulations do not reveal vortex chains intermittent with regions of regular vortex lattices as expected for anisotropic superconductors in tilted fields [10,16,17,26], which may be the result of the small simulation volume. It may be also due to our large λ approximation, which introduces long-range $1/r$ intervortex interactions instead of the exponential, $\exp(-r/\lambda)$, coupling.

Collapse and repolarization of vortices moving across the c axis involves their sharp twists around the c direction. This unusual feature may be associated with the much smaller line tension of c oriented vortex segments compared with ab segments as predicted in Ref. [8].

The above simulations do not reproduce vortex instabilities, which probably require a thorough search at different field angles and in a larger simulation volume. Also, direct account of the layered structure of YBCO is necessary for modeling the preferential entry of the normal flux along the in-plane field component, which we plan to conduct in the future.

V. CONCLUSIONS

We imaged vortex distributions in a long rectangular YBCO crystal under magnetic fields tilted from the ab plane. At small tilt angles, vortices remain in the ab plane following the predictions of the lock-in effect. With increasing field angle, the in-plane component of the flux $B_{||}$ penetrates first, followed by the normal flux component $B_\perp$, which enters anisotropically along $B_{||}$. The anisotropic $B_\perp$ entry is accompanied by the formation of modulated flux patterns, which we associate with angular vortex instabilities expected for anisotropic superconductors in tilted fields. At larger field angles the modulated flux penetration is replaced by the formation of continuous, fast moving smooth flux fronts (across $B_{||}$) and slowly entering sharp (along $B_{||}$) flux fronts of $B_\perp$. The sharp flux fronts carry enhanced currents corresponding to the rapid twist of vortices from the in-plane to the tilted direction, which occurs through the vortex cutting and reconnection process. At larger field angles and magnitudes, the anisotropy of the flux entry vanishes and the patterns transform into envelopelike structures characteristic of purely normal flux entry. We associate these changes with the crossover from the staircase to the tilted structure of vortices upon increasing the angle from the ab plane.

Our TDGL simulations confirm the advanced entry of slightly tilted vortices along the ab plane observed in the experiment. The simulations elucidate the tendency of the tilted vortices to arrange in a distorted lattice stretched along the ab plane and reveal nontrivial evolution of the vortex structure during remagnetization by tilted fields. However, closer analysis of the observed peculiarities of vortex dynamics in YBCO requires direct accounting of the layered crystal structure and will be implemented in future simulations.

ACKNOWLEDGMENTS

This paper was supported by the U.S. Department of Energy, Office of Science, Materials Sciences and Engineering Division, and Office of Advanced Scientific Computing Research, Scientific Discovery through Advanced Computing (SciDAC) program.

[1] A. A. Abrikosov, J. Phys. Chem. Solids **2**, 199 (1957).
[2] J. R. Clem, Phys. Rev. B **43**, 7837 (1991).
[3] B. I. Ivlev, Y. N. Ovchinnikov, and V. L. Pokrovskii, Mod. Phys. Lett. **5**, 73 (1991).
[4] L. N. Bulaevskii, M. Ledvij, and V. G. Kogan, Phys. Rev. B **46**, 366 (1992).
[5] G. Blatter, M. V. Feigel'mann, V. B. Geshkenbein, A. I. Larkin, and V. M. Vinokur, Rev. Mod. Phys. **66**, 1125 (1994).
[6] A. E. Koshelev, Phys. Rev. Lett. **83**, 187 (1999).
[7] A. E. Koshelev, Phys. Rev. B **71**, 174507 (2005).
[8] A. Sudbo and E. H. Brandt, Phys. Rev. Lett. **67**, 3176 (1991).
[9] L. J. Campbell, M. M. Doria, and V. G. Kogan, Phys. Rev. B **38**, 2439 (1988).
[10] A. M. Grishin, A. Yu. Martynovich, and S. V. Yampol'skii, Zh. Eksp. Teor. Fiz. **97**, 1930 (1990) [Sov. Phys. JETP **70**, 1089 (1990)]; A. M. Grishin, A. Y. Matynovich, and S. V. Yampol'skii, Physica B **165-166**, 1103 (1990).
[11] A. I. Buzdin and A. Y. Simonov, Physica C **167**, 388 (1990); **175**, 143 (1991).
[12] W. A. M. Morgado, M. M. Doria, G. Carneiro, and I. J. De Oliveira, Int. J. Mod. Phys. B **16**, 1307 (2002).
[13] A. Sudbo, E. H. Brandt, and D. A. Huse, Phys. Rev. Lett. **71**, 1451 (1993).

[14] D. Feinberg and C. Villard, Phys. Rev. Lett. **65**, 919 (1990).
[15] W. Barford and M. Harrison, Phys. Rev. B **50**, 13748 (1994).
[16] A. I. Buzdin and A. Y. Simonov, Physica C **168**, 421 (1990).
[17] V. G. Kogan, Phys. Rev. B **42**, 2631 (1990).
[18] L. L. Daemen, L. J. Campbell, A. Y. Simonov, and V. G. Kogan, Phys. Rev. Lett. **70**, 2948 (1993).
[19] E. Sardella and M. A. Moore, Phys. Rev. B **48**, 9664 (1993).
[20] G. Preosti and P. Muzikar, Phys. Rev. B **48**, 9921 (1993).
[21] M. Benkraouda and J. R. Clem, Phys. Rev. B **53**, 438 (1996).
[22] A. K. Nguyen and A. Sudbo, Phys. Rev. B **53**, 843 (1996).
[23] A. M. Thompson and M. A. Moore, Phys. Rev. B **55**, 3856 (1997).
[24] P. Muzikar, J. Low Temp. Phys. **115**, 135 (1999).
[25] E. H. Brandt, Rep. Progr. Phys. **58**, 1465 (1995).
[26] S. J. Bending and M. J. W. Dodgson, J. Phys.: Condens. Matter **17**, R955 (2005).
[27] V. Vlasko-Vlasov, A. Koshelev, A. Glatz, C. Phillips, U. Welp, and W. Kwok, Phys. Rev. B **91**, 014516 (2015).
[28] V. K. Vlasko-Vlasov, U. Welp, G. W. Crabtree, and V. I. Nikitenko, in *Physics, and Materials Science of Vortex States, Flux Pinning, and Dynamics, NATO Advanced Study Institute, Series E: Applied Sciences* Vol. 356, edited by R. Kossowsky, S. Bose, V. Pan, and Z. Durusoy (Kluwer, Dordrecht, 1999), pp. 205–237.
[29] L. M. Fisher, A. V. Kalinov, S. E. Savel'ev, I. F. Voloshin, and V. A. Yampol'skii, Physica C **309**, 284 (1998).
[30] R. Liang, D. A. Bonn, W. N. Hardy, and D. Broun, Phys. Rev. Lett. **94**, 117001 (2005).
[31] P. H. Kes, J. Aarts, V. M. Vinokur, and C. J. van der Beck, Phys. Rev. Lett. **64**, 1063 (1990).
[32] M. Beleggia, G. Pozzi, A. Tonomura, H. Kasai, T. Matsuda, K. Harada, T. Akashi, T. Masui, and S. Tajima, Phys. Rev. B **70**, 184518 (2004).
[33] L. Luan, O. M. Auslaender, D. A. Bonn, R Liang, W. N. Hardy, and K. A. Moler, Phys. Rev. B **79**, 214530 (2009).
[34] J. R. Clem, Phys. Rev. Lett. **38**, 1425 (1977).
[35] E. H. Brandt, J. Low Temp. Phys. **44**, 33 (1981); **44**, 59 (1981).
[36] Y. A. Genenko, Phys. Rev. B **51**, 3686 (1995); **53**, 11757 (1996).
[37] V. K. Vlasko-Vlasov, J. R. Clem, A. E. Koshelev, U. Welp, and W. K. Kwok, Phys. Rev. Lett. **112**, 157001 (2014).
[38] G. P. Mikitik and E. H. Brandt, Phys. Rev. B **69**, 134521 (2004).
[39] E. H. Brandt, Phys. Rev. Lett. **68**, 3769 (1992).
[40] V. K. Vlasko-Vlasov, U. Welp, G. W. Crabtree, D. Gunter, V. Kabanov, and V. I. Nikitenko, Phys. Rev. B **56**, 5622 (1997).
[41] V. K. Vlasko-Vlasov, U. Welp, G. W. Crabtree, D. Gunter, V. V. Kabanov, V. I. Nikitenko, and L. M. Paulius, Phys. Rev. B **58**, 3446 (1998).
[42] I. A. Sadovskyy, A. E. Koshelev, C. L. Phillips, D. A. Karpeyev, and A. Glatz, J. Comp. Phys. (2015), doi:10.1016/j.jcp.2015.04.002.